Pergamon

Int. J. Heat Mass Transfer. Vol. 37, No. 18, pp. 2859–2869, 1994

0017–9310/94 $7.00+0.00

0017–9310(94)00127–8

Effect of jet–jet spacing on convective heat transfer to confined, impinging arrays of axisymmetric air jets

AARON M. HUBER and RAYMOND VISKANTA†

Heat Transfer Laboratory, School of Mechanical Engineering, Purdue University, West Lafayette, IN 47907-1288, U.S.A.

(*Received* 27 *September* 1993 *and in final form* 18 *April* 1994)

Abstract—The effects of jet–jet spacing (X_n/D), low nozzle–plate spacings ($H/D = 0.25$, 1.0 and 6.0) and spent air exits located between the jet orifices were studied on the magnitude and uniformity of the convective heat transfer coefficients for confined 3×3 square arrays of isothermal axisymmetric air jets impinging normally to a heated surface. Local and average Nusselt numbers are presented for Reynolds number range of 3500–20 400. The local Nusselt numbers illustrate the (non)uniformity of the heat transfer and aid in understanding the variations in the average Nusselt number. The jet–jet spacing affects the convective coefficient by varying the influence of the adjacent jet interference and fraction of the impingement surface covered by the wall jet. The addition of spent air exits increased the convective coefficient and influenced the location of the optimum separation distance. In addition, significant enhancement of the uniformity and the convective coefficients was observed at $H/D = 0.25$ and 1.0 when compared to $H/D = 6.0$.

INTRODUCTION

During materials processing and manufacturing, the heat transfer is enhanced through jet impingement for many different applications, including the tempering and shaping of glass, the annealing of metal and plastic sheets, the cooling of gas turbine blades and the drying of textiles, veneer, paper and film materials. Rapid and uniform heating or cooling of the material is necessary to ensure material quality. The high heat and/or mass transfer rates which occur in the impingement regions of the jets result in high local transport coefficients. However, a disadvantage of impingement heating or cooling can be the nonuniformity of the heat flux distribution. Crossflow and adjacent jet interaction cause variations in the heat transfer performance of individual jets in an array which can affect the quality and/or performance of the product [1, 2].

Metzger and Korstad [3], Obot and Trabold [4] and others have shown that crossflow caused by the spent air exiting radially outward from the edges of an array decreases the magnitude and the uniformity of the convective coefficient. The crossflow and adjacent jet interference degradation of the coefficient can be minimized by having the spent air exit through openings in the orifice plate and the uniformity and magnitude of the coefficient is enhanced for the entire array. With the possibility of a very large number of jet orifices in each array, the geometry of the spent air exit significantly affects the performance of the impinging jet array. To help ensure product quality and performance through large and uniform heat transfer coefficients, it is important to understand the fluid flow and heat transfer characteristics of impinging gaseous jets.

Research during the past four decades on impinging gas jet heat transfer has led to a large body of literature. This literature has been reviewed by Livingood and Hrycak [5], Martin [1], Downs and James [6], Jambunathan *et al.* [7] and Viskanta [2]. However, the majority of the publications deal with cool turbulent air jets impinging normally onto a heated flat plate at large nozzle–plate spacings ($H/D > 1$) with or without crossflow. The available literature for axisymmetric impinging gas jet systems which is relevant to materials processing and manufacturing and not to gas turbine blade or electronic cooling is limited, with no known literature addressing the issue of axisymmetric air jet arrays with spent air exits located between the jets and/or nozzle–plate spacings smaller than 0.5 diameters.

Hollworth and Dagan [8] examined arrays of impinging jets with spent air removal through the impingement surface. They found that, for arrays with staggered (not lined up with the jet orifices) spent air exit holes, the convective coefficients were 20–30% larger than for arrays with a crossflow spent air exit geometry. However, for many material processing and manufacturing applications it is not possible to have the spent air exit through the impingement surface. Thus, spent air exhaust through the jet orifice plate is

† Author to whom correspondence should be addressed.

NOMENCLATURE

A_f	jet exit area to heat transfer area ratio, $(\pi/4)(D/X_n)^2$	q_{conv}	convective heat flux [W m^{-2}]
A_o	jet exit area to heat transfer area ratio for $X_n/D = 6$	Re_D	Reynolds number based on jet diameter, $4M/(\pi D\mu)$
D	jet diameter [m]	r	radial distance from stagnation point of jet [m]
G	factor in Martin [1] correlation	S	distance from jet centerline to spent air exit centerline for slot jets [m]
H	distance from jet exit to impingement surface [m]	T_{jet}	jet exit temperature [K]
K	factor in Martin [1] correlation	T_w	liquid crystal (impingement surface) temperature [K]
k	thermal conductivity of air at jet exit [W m^{-1} K^{-1}]	X_n	spacing between jets in a square array [m] (see Fig. 2)
l	thickness of the orifice plate [m]	x	distance along impingement surface [m] (see Fig. 2)
M	mass flow rate of air [kg s^{-1}]	y	distance along impingement surface [m] (see Fig. 2)
Nu_D	local Nusselt number based on jet diameter, hD/k	μ	air viscosity at jet orifice exit [N s m^{-2}].
$\overline{Nu}_D$	average Nusselt number based on jet diameter, $\bar{h}D/k$		

required to avoid crossflow degradation of the heat transfer coefficient.

This paper examines the effect of the jet–jet spacing ($X_n/D = 4$, 6, 8), separation distance ($H/D = 6$, 1, 0.25), Reynolds number (3500–20 400) and the presence of spent air exits located between the jet orifices in the jet orifice plate on the local Nusselt number distributions for axisymmetric confined air jet arrays. The knowledge gained from the local distributions is then used to understand the behavior of the observed average Nusselt numbers. The experimental data is also compared with the results of other investigators.

EXPERIMENTAL METHODS

Experimental apparatus

A thermochromatic liquid crystal technique was used to visualize and measure isotherms on the impingement surface [9]. Several researchers [10–13] have used liquid crystals to determine the convective heat transfer coefficients for various flow geometries. Den Ouden and Hoogendoorn [10], Goldstein and Timmers [11] and Baughn *et al.* [13] used a specific color to determine the surface temperature with human color sensation for jet impingement studies. This method involves a large amount of manual labor and relies on human color sensation, which varies between individuals. Therefore, it is subject to error and limited reproducibility. Akino *et al.* [12] eliminated the uncertainty involved with human color sensation by using bandpass filters and a video imaging system to select specific wavelengths of reflected light and thus determine the surface temperature for flow along a flat plate with a short attached cylinder. This basic technique was employed to obtain the experimental data presented in this paper.

The experimental apparatus (Fig. 1) was constructed to enable a wide range of conditions and geometries to be examined. Before entering the experimental apparatus, the air is dried and filtered, while a combination of two turbine flow meters permit measurement of a large range of flow rates (i.e. Reynolds numbers). Then, after passing through the regulator, turbine flow meters and heater, the dry air flows into the rectangular plenum chamber (25.4 cm wide, 25.4 cm deep and 36.2 cm high) and is calmed. About 100 mm from the top of the plenum, the air flows through a stainless steel mesh screen and a 51 mm thick honeycomb flow straightener which helps to ensure uniform flow from the jet orifices.

The orifices are square-edged with a 1.5 l/D ratio and diameter of 6.35 mm. The inlet of each orifice was

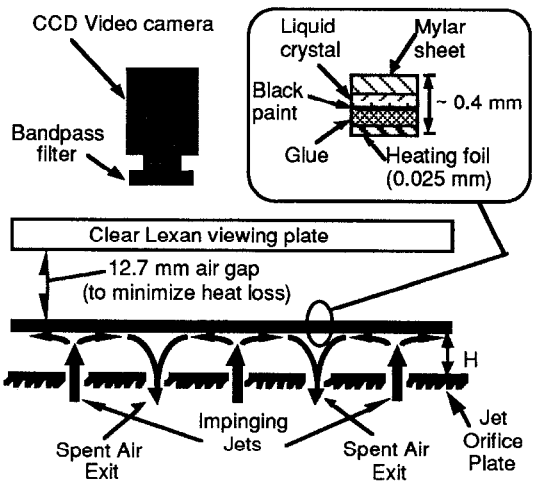

Fig. 1. Schematic diagram of orifice plate with spent air exits and impingement surface.

slightly rounded to ensure similar entrance conditions for each orifice. The orifice plate is 9.5 mm thick and 254 mm square. Thermocouples inside the plenum monitor the air temperature. Because of the low Mach number (0.14 maximum), the plenum air temperature is virtually identical to the jet exit temperature ($T/T_0 = 0.9961$ for isentropic flow at Mach = 0.14). Thus, the average plenum air temperature is used for the jet exit temperature. However, this assumption is one reason that the uncertainty in the jet exit temperature is the largest source of uncertainty in the Nusselt number.

An impingement surface similar to that shown in Fig. 1 was constructed to observe and measure the distribution of the convective heat transfer coefficient over the entire area of the surface for single and multiple isothermal jets. The impingement surface was held in tension by compressed springs over a Lexan frame. The temperature measurements using liquid crystals provide information on the heat transfer coefficient distribution as well as its magnitude. Without the use of the liquid crystal it would be very difficult to obtain even rough estimates of the local heat transfer coefficient over an area of any substantial size.

The jet orifice plates and plenum shown in Fig. 1 were mounted on a stand which allowed vertical movement. To change the separation distance, the locking bolts were loosened and the plenum and orifice plate moved upwards or downwards with an attached screw jack. To ensure accurate spacing, aluminum blocks were machined to within a ± 0.012 mm tolerance and used to check the spacing between the jet orifice plate and the impingement surface.

For this study, 3×3 square isothermal jet arrays were used with $X_n/D = 4$, 6 and 8. A 3×3 array was chosen because the center jet is completely surrounded by adjacent jets, similar to an individual jet in a large array which is not located on the perimeter. Also, the use of only nine total jets resulted in a smaller required impingement area and larger Reynolds number range. A value of $X_n/D = 6$ was recommended by Freidman and Mueller [14] to reduce adjacent jet interference and maximize heat transfer over the surface, while Martin [1] recommended an optimum value of roughly 7 diameters for $H/D = 5.4$. Thus, X_n/D values of 4, 6 and 8 were chosen to provide understanding of the Nusselt number trends above and below $X_n/D = 6$.

Figure 2 illustrates the arrangement of the orifices and spent air exit holes on the orifice plate. The impingement surface and orifice plate are of sufficient size to eliminate end effects and are open to the atmosphere on all four sides. Thus, when the spent air exit holes are closed, the spent air exits in a crossflow geometry from the four sides of the impingement surface. The spent air exit holes in the orifice plate access rectangular channels (9.5×6.3 mm) machined through the length of the orifice plate. These channels vent the spent air to the atmosphere through the sides of the orifice plate. The unit cell for the center jet is

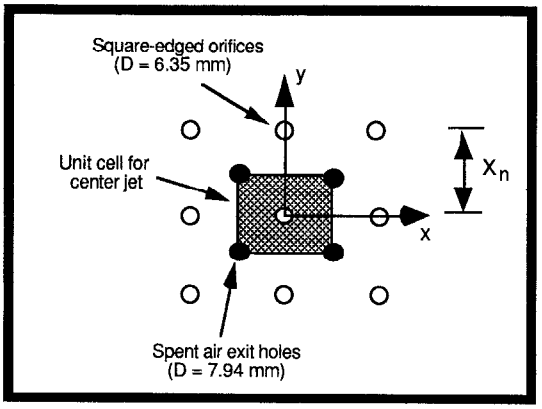

Fig. 2. Top view of the jet orifice plate showing the spent air exit ports and center jet unit cell.

also shown. This unit cell is the total impingement surface area cooled by the center jet and the ratio of the jet exit area to this surface area is the dimensionless open area, A_f. The experimental measurements were taken over the area of this unit cell for the center jet. The center jet is representative of each individual jet in an array without crossflow which is not located on the edge of the array. Jets located on the boundary or edge of an array do not have adjacent jet interference on all sides and thus exhibit slightly different behavior.

Experimental procedure

Before the experimental tests were conducted, the flow meters and bandpass filters were calibrated. The bandpass filters were calibrated by placing the liquid crystal assembly on a flat aluminum plate instrumented with thermocouples embedded near the surface, 12.7 mm apart. A constant temperature cold plate was placed at each end of the insulated aluminum plate. The temperature at each end of the aluminum plate was then varied to establish a linear temperature gradient along the length of the plate and the stainless steel impingement surface within the working temperature range of the liquid crystal.

The liquid crystal surface was viewed through the clear Lexan plate with the bandpass filters. Then the location of the isotherm indicated by the bandpass filter was matched with the temperature on the impingement surface recorded by the thermocouples. This eliminated errors in measuring the impingement surface temperature from the backside and resulted in a less than 0.1°C uncertainty in the impingement surface temperature. This small uncertainty was achieved using the bandpass filters and a liquid crystal sheet with a narrow 1°C working range. The typical temperature difference between the impingement surface temperature and the jet exit temperature was about 13°C. In addition, because the stainless steel foil impingement surface was very thin (0.0254 mm) a simple numerical estimation of the impingement assembly showed that the heat transfer could be mod-

eled as one-dimensional through the stainless steel heater and liquid crystal layer.

The heat transfer measurements were made by recording the isotherm indicated by a bandpass filter with a video camera. Simultaneously, the electrically imposed heat flux (voltage drop times the current across the heater), air flow rate, jet exit temperature and ambient temperature were measured. Approximately 20 isotherms were recorded for every 25.4 mm distance. The recorded isotherms were then digitized with an EPIX (Northbrook, IL) digitizing board and software and a PC, using 80 pixels per 25.4 mm in the horizontal direction. The individual digitized images were processed and the intensity value of each pixel depicting the location of the isotherm was set equal to the calculated local Nusselt number. The local Nusselt number for each isotherm was determined from

$$Nu_D = \frac{q_{\text{conv}} D}{(T_w - T_{\text{jet}})k}. \quad (1)$$

The jet exit temperature was used in defining the Nusselt number rather than the adiabatic wall temperature [15] for several reasons. Firstly, because the jet exit temperature was approximately equal to the ambient air temperature which minimized entrainment effects; secondly, the Reynolds numbers used in this study were low enough to avoid significant compressibility effects (maximum Mach number of 0.14); and thirdly, for design purposes the jet exit temperature is a more convenient temperature with which to work. The convective heat flux was determined from the total electric power input rate minus the estimated heat losses.

The heat losses were a combination of radiation from the heater surface and conduction losses through the top of the impingement surface assembly. Tests were conducted in the absence of jet impingement (no air flow) to obtain an estimate of the heat losses. These tests involved natural convection, radiation from the impingement surface and conduction losses through the impingement surface assembly. The tests indicated that the heat losses during jet impingement were less than 3% of the total electric power input.

After each individual isotherm image had been processed, the individual images were superimposed to create a surface map of the isotherms. Using commercial computer software (PV-WAVE produced by Precision Visuals, Boulder, CO) the surface isotherm map was converted to a uniform two-dimensional array of local Nusselt numbers, with each pixel from the isothermal image (7200 pixels for the $X_n/D = 6$ unit cell) corresponding to one array entry. Various plots and slices of the data were then obtained to gain understanding of the local heat transfer coefficient over the entire unit cell surface.

Using a 95% confidence level, the uncertainty in the Nusselt and Reynolds numbers was determined with a root–sum–square method [16]. The Nusselt number calculation had an uncertainty range of 4–9%, while the uncertainty in the Reynolds number calculation was estimated to be 3.2%. The results were reproducible within these uncertainty ranges.

RESULTS AND DISCUSSION

Local heat transfer

The three-dimensional plot (Fig. 3) illustrates the symmetry of the local heat transfer coefficient around the stagnation point for the $X_n/D = 6$ unit cell area. Thus, two-dimensional plots of the radial Nusselt number distributions can be used for comparison. Figure 3 is for $H/D = 1$, which Metzger *et al.* [17], Hrycak [18] and Ichimiya and Okuyama [19] have reported as the approximate distance for the maximum average heat transfer coefficient with an array of axisymmetric air jets ($H/D < 0.5$ distances were not studied by the above investigators). Examination of the Nu_D values of Fig. 3 clearly show the presence of secondary rings or peaks and indicate that these secondary rings increase the average convection coefficient. Thus, the maximum Nu_D no longer occurs at the stagnation point as observed with larger separation distances, but at secondary rings around the stagnation point. These rings occur at $r/D \approx 0.5$ and $r/D \approx 1.6$.

Prior researchers have discussed and provided explanations for the occurrence of these secondary peaks with single unconfined jets. The inner peak, which occurred at $r/D \approx 0.5$, is attributed to both the fluid accelerating out of the stagnation region which thins the local boundary layer and the influence of the shear layer generated turbulence around the circumference of the jet by various investigators [9]. There is agreement among several authors [10, 20–22] that the inner secondary peak becomes less pronounced as the Reynolds number is reduced and the separation distance is increased. However, due to the differing nozzle geometry and flow conditions, the separation distance where the peak disappeared varied between the studies.

The outer secondary peak was shown by den Ouden and Hoogendoorn [10] and Lytle and Webb [20] to be caused by the transition to turbulent flow in the boundary layer. Thus, as the Reynolds number increases, the outer peak in the local Nusselt number becomes more pronounced. A decrease in the Reynolds number or the separation distance appears to promote an earlier boundary layer transition from laminar to turbulent flow, because the location of the outer peak moves toward the stagnation point when either of these two parameters are varied appropriately.

Effect of jet–jet spacing (X_n/D). In this section, the Nu_D distributions are compared for a single impinging jet of similar geometry and the center jet of the 3×3 square jet arrays as H/D is varied. The local convective coefficients for $H/D = 6.0$ and $Re_D = 10\,300$ are plotted in Fig. 4. The values for the single jet with a Reynolds number of 6900 are also shown in the figure for the purpose of comparison. At $H/D = 6.0$, roughly equal to the length of the potential core, the Nusselt

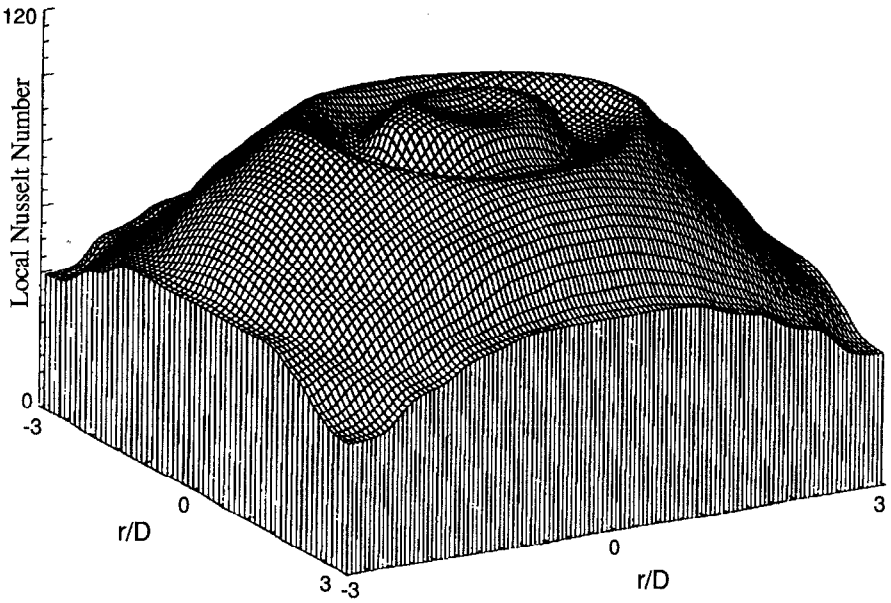

Fig. 3. Local Nusselt number distribution for $H/D = 1.0$, $X_n/D = 6$ and $Re_D = 17\,100$.

number is a maximum at the stagnation point and decreases as r/D increases. While all the Nu_D distributions exhibit the same behavior, there is a significant difference in the magnitude of Nu_D between the single jet and the jet arrays. At the same Re_D, the Nusselt numbers for the jet arrays are 14–21% lower at the stagnation point than the values for the single jet. In fact, the local Nusselt numbers for the single jet are nearly identical to the values for $X_n/D = 8$ and larger in magnitude than the results for $X_n/D = 6$ and 4. This follows the trend reported in the literature, as Hollworth and Berry [23] and Hrycak [18] both note that the average heat transfer coefficient for a single jet is greater than that for a given jet of equivalent geometry in an array. Both articles attribute the decrease in the convection coefficient to adjacent jet interaction (before impingement and in the wall jet region) and the exit of spent air (including crossflow).

For the experimental data, only the local convective coefficients obtained with open spent air exits were compared to the single jet convective coefficient distributions. Therefore, the effects of crossflow and the adjacent jet interference in the wall jet region are minimized. Hence, it appears that the major degradation of the convection coefficient for the jets in an array is due to adjacent jet interactions which occur before impingement. These interactions increase the decay of the jet velocity, increase entrainment of surrounding air and influence the ring vortices located around the jet circumference which affect the turbulent mixing associated with the shear layer [24, 25]. The figure shows that degradation due to adjacent jet interactions before impingement occur as the local Nusselt numbers for the single jet at $Re_D = 6900$ are nearly identical with the local Nusselt numbers for the $X_n/D = 8$ array jet at $Re_D = 10\,300$.

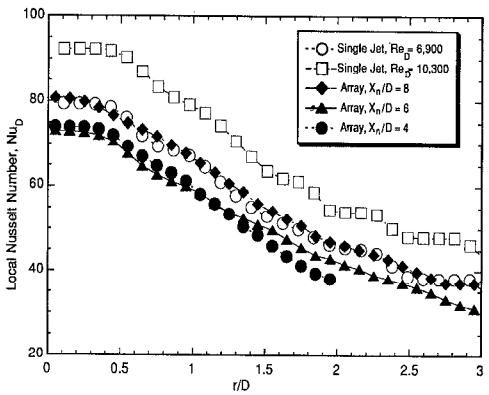

Fig. 4. Effect of jet–jet spacing on the local Nusselt numbers for $H/D = 6.0$ and $Re_D = 10\,300$.

The influence of the adjacent jet interference should decrease with an increasing jet–jet spacing. This expected trend is also shown in Fig. 4, as the $X_n/D = 8$ array has higher local Nusselt numbers than the $X_n/D = 6$ or 4 arrays. This trend is not clearly evident with the $X_n/D = 6$ and 4 arrays. The $X_n/D = 4$ array has a slightly higher local Nusselt number at the stagnation point than the $X_n/D = 6$ array, but the Nu_D distribution for $X_n/D = 4$ then crosses over the $X_n/D = 6$ distribution at about $r/D = 1.1$–1.2 and becomes smaller. However, the Nu_D values for $X_n/D = 6$ and 4 are lower than those for $X_n/D = 8$ and the $Re_D = 6900$ single jet.

Figure 5 further illustrates these trends for a larger Re_D of 17 100 for the three arrays. Once again, the local convective coefficients for the jet arrays are comparable to the local convective coefficients for the single impinging jet with significantly lower Reynolds numbers (mass flow rates). In fact, the Nu_D distributions for the jet arrays with $Re_D = 17\,100$ are bracketed between the $Re_D = 13\,700$ and 10 300 dis-

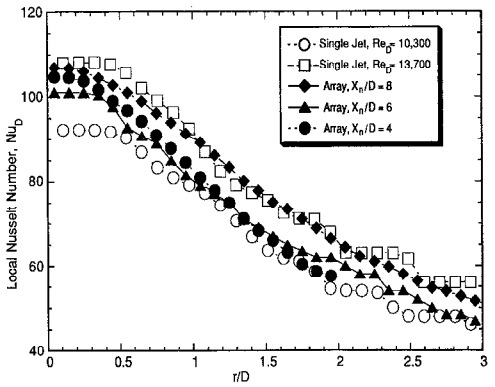

Fig. 5. Effect of jet–jet spacing on the local Nusselt numbers for $H/D = 6.0$ and $Re_D = 17\,100$.

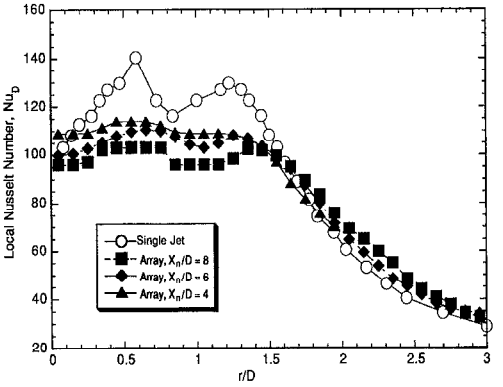

Fig. 7. Effect of jet–jet spacing on the local Nusselt numbers for $H/D = 0.25$ and $Re_D = 10\,300$.

tributions for the single jet. This again depicts the significant degradation of the local convective coefficient by adjacent jet interactions which occur before impingement. As with Fig. 4, the Nusselt numbers for the $X_n/D = 8$ array are larger in magnitude than the results for the $X_n/D = 6$ and 4 arrays and the values for the $X_n/D = 6$ and 4 arrays cross over each other at about $r/D = 1.2$..

Figure 6 shows the distributions for $Re_D = 10\,300$ and $H/D = 1.0$. At this smaller separation distance, the adjacent jet interactions which occur before impingement are strongly reduced due to the smaller distance for the interactions to occur. This is evidenced by the fact that, for the identical Re_D, the single jet Nu_D values now agree well with those for the three jet arrays. No longer is there a significant difference between the local convective coefficients for the single jet and the local convective coefficients for the three arrays. There is only a slight difference in the magnitude of the inner peak. This difference is probably due to the presence of a small flow resistance caused by the surrounding jets in the array which slightly decreases the acceleration of the fluid out of the stagnation region. This results in a thicker boundary layer and thus lower local convective coefficients for the jet arrays in the inner secondary peak region. Because this flow resistance should be smallest for the

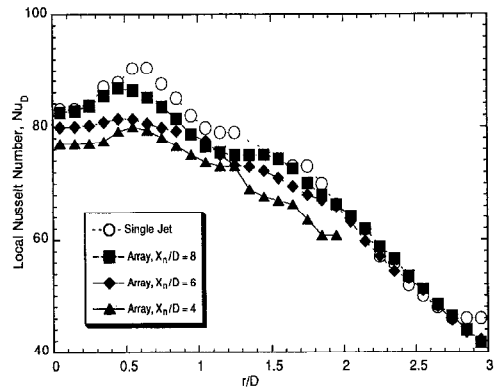

Fig. 6. Effect of jet–jet spacing on the local Nusselt numbers for $H/D = 1.0$ and $Re_D = 10\,300$.

$X_n/D = 8$ array, the local Nusselt numbers should agree better with the single jet local Nusselt numbers than the other two arrays. Figure 6 shows that the local Nusselt numbers for the $X_n/D = 8$ array do agree with the results for the single jet better than the data for the $X_n/D = 6$ and $X_n/D = 4$ arrays. However, in the wall jet region the local Nusselt numbers for all the arrays overlap and merge together.

Figure 7 depicts the Nu_D distributions for $H/D = 0.25$ and $Re_D = 10\,300$. As with $H/D = 1.0$, the single jet data and array jet data agree well at the stagnation point and wall jet region. However, the distributions for the single jet and the array jets in the location of the secondary peaks reveal significant differences. The secondary peaks for the single jet are more pronounced than the secondary peaks for the jet array distributions. As the Reynolds number is increased, this difference between the arrays and single jet increases. Apparently, the influence of the adjacent jets in the arrays dampens out the secondary peaks and creates a more uniform Nusselt number distribution. Also, with $H/D = 0.25$, the secondary peaks, especially the outer peak, are more pronounced than at $H/D = 1.0$. This is especially true for the single jet.

The three arrays exhibit another difference between the distributions at $H/D = 0.25$ and the distributions at $H/D = 1.0$ and 6.0. At the two larger separations distances, Nu_D for $X_n/D = 8$ was always the largest and agreed the best with the results for the single jet. Now, at $H/D = 0.25$, it is the smallest in magnitude and exhibits the largest difference in comparison with the single jet Nu_D. This was not expected, as $X_n/D = 8$ should result in smaller adjacent jet interactions than for $X_n/D = 6$ and 4 and thus have smaller differences between the single jet and the center jet in the array. Similar to the behavior at $H/D = 1.0$ and 6.0, the distributions for $X_n/D = 4$ and 6 agree very well with each other. For $H/D = 0.25$, the Nusselt numbers for $X_n/D = 4$ tend to be slightly larger in magnitude than those for $X_n/D = 6$ at most of the Reynolds numbers.

Effect of spent air exits. At $H/D = 1$, the presence of spent air exits have no observable effect on the local Nusselt number distributions. This is because the gap

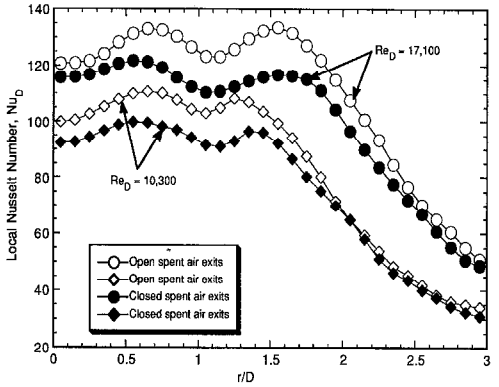

Fig. 8. Local Nusselt numbers with and without spent air exits for $H/D = 0.25$ and $X_n/D = 6.0$.

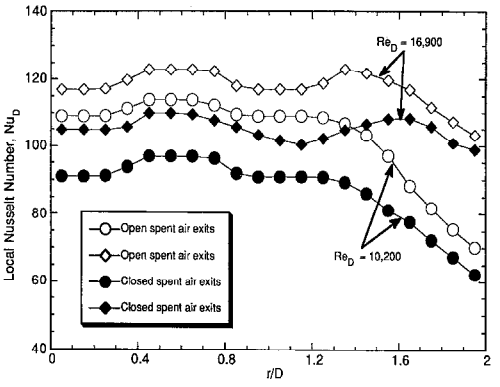

Fig. 9. Local Nusselt number with and without spent air exits for $H/D = 0.25$ and $X_n/D = 4.0$.

between the impingement surface and confining jet orifice plate is large enough to channel the flow outward without a significant pressure drop. Also, because the jet used for the measurements is the center jet of a 3×3 array, all of the flow is radially outward and thus, even with the spent air exits blocked, there is no crossflow to degrade the convective coefficient. In a large array, crossflow and flow channeling can have a significant effect on both the uniformity and magnitude of the heat transfer coefficient [3–6, 26]. These effects should be minimized by placing spent air exits between the jet orifices in the jet orifice plate; however, the small array used in this study does not experience crossflow and flow channeling. Thus, for a large array, a difference in the heat transfer coefficients for the closed and open spent air exits would be expected at $H/D \geqslant 1$.

When H/D is decreased to 0.25, there is a difference between the Nusselt numbers with and without the spent air exits. This is shown in Fig. 8 for the $X_n/D = 6$ with two Reynolds numbers. The narrower gap between the impingement surface and the confining jet orifice plate results in a resistance to the flow which, with no spent air exits, must exit radially outward. This resistance to the flow degrades the convective coefficient. With no spent air exits, the boundary layer transition also appears to be delayed as the outer secondary peak occurs at a larger r/D value for the case of no spent air exits than with spent air exits in the orifice plate. Once again, the presence of crossflow for the arrangement with no spent air exits would have degraded the convective coefficient and increased the difference between the two cases.

The effect of the spent air exits on the Nu_D distributions is greater at $X_n/D = 4$. Here, the closer jet–jet spacing causes larger flow restrictions and adjacent jet interactions. Because the fluid has less impingement surface area (smaller unit cell) before contacting the adjacent wall jets to spread out and slow down for $X_n/D = 4$ than for the other arrays, the momentum of the fluid is higher when contact is made with the adjacent wall jets. This higher momentum strongly influences the adjacent jet interactions and causes a larger flow resistance. Thus, the difference between the distributions with and without spent air exits shown in Fig. 9 is larger than for those shown in Fig. 8 for $X_n/D = 6$. The closer jet–jet spacing means that, for the same jet Re_D, the mass flux is higher (i.e. $X_n/D = 6$ has a unit cell area for the center jet 2.25 times larger than $X_n/D = 4$ and $X_n/D = 8$ has a unit cell area 4.0 times larger than $X_n/D = 4$). The higher mass flux increases the flow interactions and degrades the convective coefficient due to crossflow unless well-designed spent air exits are used.

From Fig. 10, it is seen that the difference between the Nu_D distribution with spent air exits and the distribution without spent air exits is small. This figure is for the largest X_n/D of 8 and therefore the largest impingement surface area per jet. The smaller mass flux for this array reduces the adjacent jet interactions and, without the presence of crossflow, results in small differences between the Nusselt number distributions with and without spent air exits.

The reported results depict the importance of spent air exits with small separation distances. The additional minimization of crossflow heat transfer coefficient degradation means that a significant enhancement of convective coefficient can occur through the use of spent air exits. The uniformity of the convective coefficient across the array is also

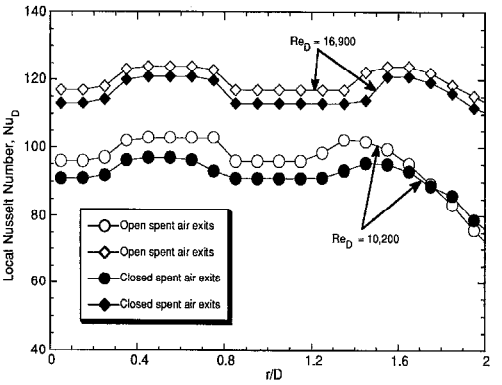

Fig. 10. Local Nusselt number with and without spent air exists for $H/D = 0.25$ and $X_n/D = 8.0$.

Table 1. Approximate axisymmetric S/H values for test conditions, where S is the radial distance between the axisymmetric jet and spent air exit

H/D	S/H ($X_n/D = 4$)	S/H ($X_n/D = 6$)	S/H ($X_n/D = 8$)
6.0	0.47	0.71	0.94
1.0	2.83	4.24	5.66
0.25	11.31	16.97	22.6

improved as each individual jet's unit cell has nearly identical flow conditions and Nu_D distributions. Uniformity of the local heat transfer coefficient is important for the material processing applications for which these types of arrays are used.

Saad *et al.* [27] examined the effect of the relative distance from the jet centerline to the centerline of the spent air exit (S/H) for multiple impinging slot jets. While there are differences between the two-dimensional flow of slot jets and the three-dimensional flow of axisymmetric orifices, the general trends are applicable. They found that a multiple slot jet could be classified as interacting (i.e. significant adjacent jet interference) or noninteracting, according to whether S/H was less than or greater than 1.5. Unfortunately, unlike slot jets, axisymmetric jets do not have a simple and clearly defined distance from the center of the jet to the center of the spent air exits, because the axisymmetric jet is not completely surrounded by spent air exits (see Fig. 2). However, for discussion, S/H values for the axisymmetric jets are presented in Table 1 using the radial distance between the centers of the jet and spent air exit. Using the finding of Saad *et al.* [27] for slot jets that, with $S/H > 1.5$, adjacent jet interactions are minimal, it can be seen from Table 1 that, for $H/D = 6.0$, adjacent jet interference should be significant. As H/D was decreased to 1.0 and 0.25, S/H increased above 1.5. This suggests that an individual jet in the array acted more like a single jet with no or little adjacent jet interference. These trends were evident from the experimental data and the observations reported by Saad *et al.* agree with the discussion of Figs. 4–7.

Average Nusselt number

The three-dimensional plots of the local Nusselt number were averaged over the square unit cell area [9]. In an array with spent air exits, the Nu_D distribution should be similar for each unit cell; therefore, $\overline{Nu_D}$ for the unit cell is the average for the entire array. A comparison of $\overline{Nu_D}$ values for the three jet–jet spacings is given in Fig. 11. For clarity, only $H/D = 6.0$ and 1.0 are plotted. It is clear that $\overline{Nu_D}$ values for a given Re_D and H/D are largest for $X_n/D = 4$. The average Nusselt numbers for $X_n/D = 6$ are then next highest, with those for $X_n/D = 8$ being the lowest. For $H/D = 6.0$, which is at the end of the potential core region, the local maximum Nusselt number occurs in the stagnation point region, which

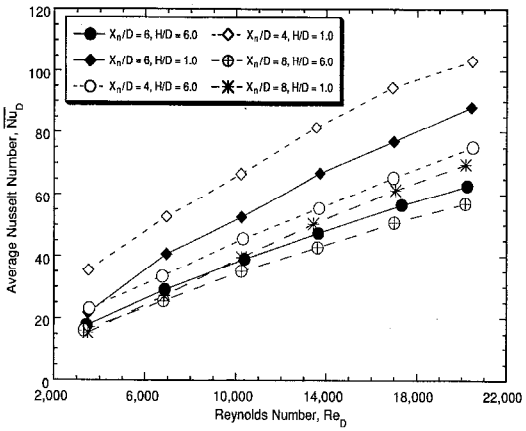

Fig. 11. Comparison of average Nusselt numbers for $X_n/D = 4$, 6 and 8 at $H/D = 6.0$ and 1.0.

occupies a small fraction of the total area. However, when the separation distance is decreased to $H/D = 1.0$, there is a considerable enhancement of $\overline{Nu_D}$. This is due to the secondary maximum peaks in the local Nusselt number. These secondary peaks occur as rings which significantly increase the surface area where the local Nusselt numbers are high. The dependence on the Re_D is also strengthened because of the relationship between the secondary peaks and the Reynolds number. At the low Re_D of 3500, the difference between the $\overline{Nu_D}$ for $H/D = 6.0$ and 1.0 is small, because the secondary peaks are virtually nonexistent at this value. But, as the Re_D is increased, the secondary peaks appear and become more pronounced for $H/D = 1.0$. Thus, the average Nusselt number becomes significantly higher than for $H/D = 6.0$.

While the $X_n/D = 4$ array has the largest heat transfer coefficients, it also has the highest mass flow rate per unit surface area. The unit cell area for $X_n/D = 6$ is 2.25 times larger than the area of the unit cell for $X_n/D = 4$ and the unit cell area for $X_n/D = 8$ is 4 times larger than the unit cell area for $X_n/D = 4$. This means that, while the unit cell area for $X_n/D = 8$ is covered by just one impinging jet, an equivalent area for $X_n/D = 4$ is covered by four impinging jets and thus experiences four times the mass flow rate of air for equivalent Re_D. Hence, for applications which require the highest possible average heat transfer coefficients, $X_n/D = 4$ would be the best choice. This is also true for uniformity of the heat transfer, which is best for $X_n/D = 4$ with spent air exits as shown by the Nu_D distributions.

For applications in which the mass flow rate is limited or is an important parameter to minimize due to cost, etc., it is not clear from Fig. 11 which array is most efficient on a mass flux basis. Therefore, $\overline{Nu_D}$ values for the three arrays were normalized by using a ratio of the open areas. The open area ratio for $X_n/D = 6$, A_o, was used as the standard for comparison and to create dimensionless ratios, A_o/A_f.

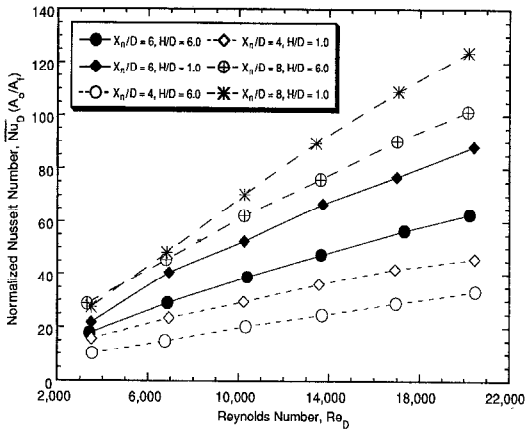

Fig. 12. Normalized average Nusselt numbers for $X_n/D = 4$, 6 and 8 at $H/D = 6.0$ and 1.0.

Hence, $\overline{Nu_D}$ values were multiplied by this ratio so that comparisons on an equivalent mass flux basis could be made between the three arrays. Figure 12 shows the results of this mass flow rate per unit surface area normalization of the average Nusselt numbers.

From Fig. 12, it is seen that, based on an equivalent mass flow rate per unit area, the $X_n/D = 8$ array performs the best and exhibits the largest $\overline{Nu_D}$ values. Because this array has the largest unit cell area, a unit mass of fluid has more contact with the surface to remove heat and thus is more efficient on a mass flux basis then the other jet–jet spacings. But, from the Nu_D distributions, the $X_n/D = 8$ array has the least uniform heat transfer coefficient distribution across the impingement surface. Therefore, a trade-off between achieving high average Nusselt numbers and minimizing the mass flow rate exists with the jet–jet spacing parameter.

The $\overline{Nu_D}$ values for $H/D = 0.25$, 1.0 and 6.0 with the open spent air exits were correlated for the three arrays, with Re_D, H/D and X_n/D as the independent variables. The correlation for the experimental data is

$$\overline{Nu_D} = 0.285 Re_D^{0.710} Pr^{0.33} (H/D)^{-0.123} (X_n/D)^{-0.725}. \quad (2)$$

The range of validity is the range of parameters for the experimental data which are: $3400 \leqslant Re_D \leqslant 20\,500$, $4 \leqslant X_n/D \leqslant 8$ $(0.0123 \leqslant A_f \leqslant 0.0491)$ and $0.25 \leqslant H/D \leqslant 6.0$. The observed trends in the experimental data are shown by the exponents of the independent parameters. The exponent for H/D is negative. For the parameters used in this study, smaller H/D values result in higher $\overline{Nu_D}$ values. The jet–jet spacing with an exponent of -0.725 has a strong impact on $\overline{Nu_D}$. This exponent occurs because, at smaller jet–jet spacings, a greater fraction of the impingement surface area is covered by the stagnation region and secondary rings with high local Nusselt numbers than at larger jet–jet spacings where a larger fraction of the impingement surface is covered by the wall jet region, where the local Nusselt numbers are low. Most of the experimental data points lie within a $\pm 10\%$ band, but a few fall outside the -10% range. However, all the data points deviate by less than 20% from the correlation.

The $X_n/D = 6$ array showed very good agreement with the correlation as all its related data points fell within the $\pm 10\%$ band, while the $X_n/D = 8$ array had the greatest scatter. The data points with the largest difference from the correlation (-10 to -20%) were those for $X_n/D = 4$ at $H/D = 6$ and $X_n/D = 8$ at $H/D = 0.25$. It is difficult to develop a simple correlation which would accurately predict the many complex trends associated with impinging jet arrays. The $X_n/D = 4$ array at $H/D = 6$ experienced the largest heat transfer degradation due to adjacent jet interactions before impingement. This was not fully accounted for by the correlation which leads to the larger overpredictions. The $\overline{Nu_D}$ enhancement by the secondary rings is weakened for $X_n/D = 8$ at $H/D = 0.25$ because the area covered by the secondary rings and stagnation region is now less than the impingement surface area covered by the wall jet. Thus, the low local heat transfer coefficients associated with the wall jet region dampen the enhancement of the secondary rings when compared with $X_n/D = 6$ and 4. Hence, the correlation overpredicts the $\overline{Nu_D}$ for $X_n/D = 8$ at $H/D = 0.25$.

The average Nusselt numbers for the three jet arrays are also compared to the correlation presented by Martin [1]. The correlation was obtained by modifying the equation for a single round nozzle, and thus Martin [1] comments that it is valid for arrays with good outlet flow conditions. He further states that when the spent air is forced to flow laterally over the width of the material (crossflow) the outlet stream may significantly influence the entire flow and temperature fields. Because the present experimental data was obtained with spent air exits and no crossflow, the Martin [1] correlation presented below should be applicable. It is of the form

$$\overline{Nu_D} = 0.5 K G Re_D^{0.667} Pr^{0.42}, \quad (3)$$

where

$$K = \left\{1 + \left(\frac{(H/D)\sqrt{A_f}}{0.6}\right)^6\right\}^{-0.05} \quad (4)$$

and

$$G = 2\sqrt{A_f}\,\frac{1 - 2.2\sqrt{A_f}}{1 + 0.2(H/D - 6)\sqrt{A_f}}. \quad (5)$$

The range of validity given for this correlation is: $2000 \leqslant Re_D \leqslant 100\,000$, $4.43 \leqslant X_n/D \leqslant 14.0$ $(0.004 \leqslant A_f \leqslant 0.04)$ and $2 \leqslant H/D \leqslant 12$. For comparison, the measured average Nusselt numbers and the average Nusselt numbers predicted by the Martin correlation were normalized by the G, K, and Prandtl number terms shown in equations (3)–(5). These normalized

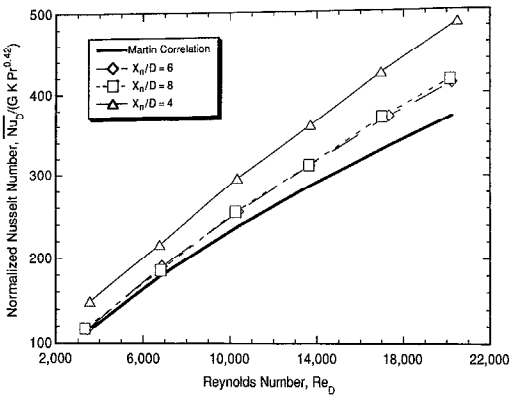

Fig. 13. Comparison of average Nusselt numbers with Martin [1] correlation for $H/D = 6.0$.

Nusselt numbers were then plotted vs the Reynolds number.

Figure 13 reveals the good agreement between the correlation and the experimental data for $H/D = 6.0$ with $X_n/D = 8$ and 6. These two arrays match the values predicted by the correlation closely at the Re_D of 3500 and 6900; but then, as Re_D increases, the difference between the correlation and the experimental data increases. The experimental data have steeper slopes than the predicted values which shows a stronger Re_D dependence. The Martin correlation has a Reynolds number exponent of 0.667, while the present experimental data has an exponent of about 0.710. The larger exponent for the experimental data could be due to the elimination of crossflow degradation by the spent air exit ports, while the Martin correlation was shown to have good agreement with arrays which experienced minimal crossflow [1, 19]. Differences in nozzle geometry and upstream flow conditions also influence the comparison. Overall, the correlation underpredicts the experimental data by less than 10% for $X_n/D = 6$ and 8. The $X_n/D = 4$ array does not exhibit very good agreement with the correlation. This is due to the limitations of the correlation. The correlation is valid only for a minimum of $X_n/D = 4.43$, so $X_n/D = 4$ is outside the valid parameter range. Thus, the increase in the adjacent jet interactions due to the smaller jet–jet spacing are not taken into account in the G and K factors of the correlation and this leads to the large (about 30%) discrepancy.

Since the Martin correlation is not valid below $H/D = 2$, comparison between the correlation and experimental data at $H/D = 1$ and 0.25 is not presented here. However, to understand better the limitations of the correlation and its application to the design of impinging jet systems, these comparisons are given elsewhere [9]. Figure 13 does show that within the valid range of parameters, the Martin correlation predicts the experimental data well. The G and K factors of the correlation collapse the data points into a simple normalized $\overline{Nu}_D$ vs Re_D relationship.

CONCLUSIONS

This paper has reported a study on convective heat transfer to confined isothermal impinging gas jet arrays to gain understanding of the physical mechanisms which affect the uniformity of the local heat transfer coefficient and the average heat transfer coefficient. It was found that, for an array jet at $H/D = 6.0$, adjacent jet interference before impingement causes significant degradation of the convection coefficient when compared to a single jet. However, as the separation distance is decreased to one jet diameter, the adjacent jet interference before impingement is minimized and the Nusselt numbers for the array jet and single jet are similar. Also, at small separation distances ($H/D \leqslant 1.0$) secondary maxima occur in the local convective coefficient for a jet in an array similar to a single jet. These secondary maxima enhance the average convective coefficients. The $X_n/D = 4$ spacing resulted in the highest average Nusselt number for a given separation distance as well as the most uniform distribution over the impingement surface. This is because a large fraction of the impingement surface is covered by the stagnation region and the influence of the low convection coefficients associated with the wall jet region are minimized. However, on a mass flux basis, the $X_n/D = 8$ array was found to be the most efficient.

Spent air exits located between the jet orifices in the jet orifice plate result in heat transfer enhancement by minimizing adjacent jet interference in the wall jet region and crossflow degradation of the convective coefficient. As the jet–jet spacing is decreased, the effect of the spent air exits on the Nusselt number increases. With spent air exits, the surface area heated or cooled by each jet in an array experiences similar conditions and thus exhibits similar performance. Therefore, the spent air exits are important in maintaining uniform heat transfer over the entire surface covered by a jet array.

REFERENCES

1. H. Martin, Heat and mass transfer between impinging gas jets and solid surfaces. In *Advances in Heat Transfer*, Vol. 13 (Edited by T. Irvine and J. P. Harnett), pp. 1–60. Academic Press, New York (1977).
2. R. Viskanta, Heat transfer to impinging isothermal gas and flame jets, *Exp. Thermal Fluid Sci.* **6**, 111–134 (1993).
3. D. E. Metzger and R. J. Korstad, Effects of crossflow on impingement heat transfer, *J. Engng Power* **94**, 35–42 (1972).
4. N. T. Obot and T. A. Trabold, Impingement heat transfer within arrays of circular jets: part 1—effects of minimum, intermediate, and complete crossflow for small and large spacings, *J. Heat Transfer* **109**, 872–879 (1987).
5. J. N. B. Livingood and P. Hrycak, Impingement heat transfer from turbulent air jets to flat plates—a literature survey, *NASA TMX*-2778 (1973).
6. S. J. Downs and E. H. James, Jet impingement heat transfer—a literature survey, ASME Paper No. 87-HT-35 (1987).
7. K. Jambunathan, E. Lai, M. A. Moss and B. L. Button, A review of heat transfer data for single circular jet impingement, *Int. J. Heat Fluid Flow* **13**, 106–115 (1992).

8. B. R. Hollworth and L. Dagan, Arrays of impinging jets with spent fluid removal through vent holes on the target surface part 1: average heat transfer, *J. Engng Power* **102,** 994–999 (1980).
9. A. M. Huber, Heat transfer with impinging gaseous jet systems, Ph.D. Thesis, Purdue University, West Lafayette, IN (1993).
10. C. den Ouden and C. J. Hoogendoorn, Local convective heat transfer coefficients for jets impinging on a plate: experiments using a liquid crystal technique, *Proc. 5th Heat Transfer Conf.*, Vol. 5, pp. 293–297. AIChE, New York (1974).
11. R. J. Goldstein and J. F. Timmers, Visualization of heat transfer from arrays of impinging jets, *Int. J. Heat Mass Transfer* **25,** 1857–1868 (1982).
12. N. Akino, T. Kunugi, K. Ichimiya, K. Mitsushiro and M. Ueda, Improved liquid-crystal thermometry excluding human color sensation, *J. Heat Transfer* **111,** 558–565 (1989).
13. J. W. Baughn, A. E. Hechanova and X. Yan, An experimental study of entrainment effects on the heat transfer from a flat surface to a heated circular impinging jet, *J. Heat Transfer* **113,** 1023–1025 (1991).
14. S. J. Freidman, and A. C. Mueller, Heat transfer to flat surfaces, *Proc. General Discussion on Heat Transfer*, Institution of Mechanical Engineers, London, pp. 138–142 (1951).
15. R. J. Goldstein, K. A. Sobolik and W. S. Seol, Effect of entrainment on the heat transfer to a heated circular air jet impinging on a flat surface, *J. Heat Transfer* **112,** 608–611 (1990).
16. R. Moffat, Describing the uncertainties in experimental results, *Exp. Thermal Fluid Sci.* **1,** 3–17 (1988).
17. D. E. Metzger, T. Yamashita and C. W. Jenkins, Improvement cooling of concave surfaces with lines of circular air jets, *J. Engng Power* **91,** 149–158 (1969).
18. P. Hrycak, Heat transfer from a row of impinging jets to concave cylindrical surfaces, *Int. J. Heat Mass Transfer* **24,** 407–418 (1981).
19. K. Ichimiya and K. Okuyama, Characteristics of impingement heat transfer caused by circular jets with confined wall, *Proc. 3rd Int. Cold Regions Heat Transfer Conf.*, pp. 523–532 (Edited by J. P. Zarling). University of Alaska–Fairbanks, AK (1991).
20. D. Lytle and B. W. Webb, Secondary heat transfer maxima for air jet impingement at low nozzle-to-plate spacings. In *Experimental Heat Transfer, Fluid Mechanics, and Thermodynamics*, pp. 776–783 (Edited by J. F. Keffer, R. K. Shah and E. N. Gánic). Elsevier Science, New York (1991).
21. R. Gardon and J. C. Akfirat, The role of turbulence in determining the heat transfer characteristics of impinging jets, *Int. J. Heat Mass Transfer* **8,** 1261–1272 (1965).
22. N. T. Obot, A. S. Mujumdar and W. J. M. Douglas, The effect of nozzle geometry on impingement heat transfer under a round turbulent jet, ASME Paper No. 79-WA/HT-53 (1979).
23. B. R. Hollworth and R. D. Berry, Heat transfer from arrays of impinging jets with large jet-to-jet spacing, ASME Paper No. 78-GT-117 (1978).
24. K. Kataoka, Impingement heat transfer augmentation due to large scale eddies, *Proc. 9th Int. Heat Transfer Conf.*, Vol. 1, pp. 255–273. Hemisphere, Washington, DC (1990).
25. S. Yokobori, N. Kasagi, M. Hirata and N. Nishiwati, Role of large-scale eddy structure on enhancement of heat transfer in stagnation region of two-dimensional, submerged, impinging jet, *Proc. 6th Int. Heat Transfer Conf.*, Vol. 5, pp. 305–310. Hemisphere, Washington, DC (1978).
26. P. Krötzsch, Heat and material transfer on impact streaming from fields of nozzles and orifices, *Chem. Ing. Tech.* **40,** 339 (1968).
27. N. R. Saad, S. Polat and W. J. M. Douglas, Confined multiple impinging slot jets without crossflow effects, *Int. J. Heat Fluid Flow* **13,** 2–14 (1992).